Variation in the Three-Dimensional Histomorphometry of the Normal Human Optic Nerve Head With Age and Race: Lamina Cribrosa and Peripapillary Scleral Thickness and Position

Christopher A. Girkin,[1] Massimo A. Fazio,[1,2] Hongli Yang,[3] Juan Reynaud,[3] Claude F. Burgoyne,[3] Brandon Smith,[1] Lan Wang,[1] and J. Crawford Downs[1]

[1]Department of Ophthalmology, School of Medicine, University of Alabama at Birmingham, Birmingham, Alabama, United States
[2]Department of Biomedical Engineering, School of Engineering, University of Alabama at Birmingham, Birmingham, Alabama, United States
[3]Devers Eye Institute, Legacy Health System, Portland, Oregon, United States

Correspondence: Christopher A. Girkin, Department of Ophthalmology, UAB Callahan Eye Hospital, 1700 South 18th Street, Suite 601, Birmingham, AL 35213, USA; cgirkin@uab.edu.

CAG and MAF contributed equally to the work presented here and therefore should be considered equivalent authors.

Submitted: March 13, 2017
Accepted: June 13, 2017

Citation: Girkin CA, Fazio MA, Yang H, et al. Variation in the three-dimensional histomorphometry of the normal human optic nerve head with age and race: lamina cribrosa and peripapillary scleral thickness and position. *Invest Ophthalmol Vis Sci.* 2017;58:3759–3769. DOI:10.1167/iovs.17-21842

Purpose. This study quantified the thickness and depth of the lamina cribrosa (LC) and peripapillary scleral thickness in high-resolution three-dimensional (3D) fluorescent reconstructions of the optic nerve head (ONH) in eyes from donors of African (AD) and European descent (ED).

Methods. A total of 64 eyes (45 ED, 19 AD) from 51 normal donors were obtained within 6 hours of death and fixed at 10 mm Hg of pressure. The optic nerve head was trephined from the globe and digitally reconstructed at 1.5 × 1.5 × 1.5 μm voxel resolution with an automated episcopic fluorescence technique. The load-bearing ONH connective tissue surfaces were manually delineated in 3D using custom software.

Results. The lamina cribrosa and peripapillary sclera were significantly thinner in AD eyes adjusting for age and sex (LC was 24 ± 11 μm thinner; $P = 0.0350$; scleral was 56 ± 22 μm thinner; $P = 0.0097$). The lamina cribrosa was significantly thinner in females (23 ± 11 μm thinner; $P = 0.0425$). Age was not significantly associated with any morphologic parameter in the ED group. However, increasing age was associated with an increase in scleral thickness (1.3 μm/year, $P = 0.0499$) and an increase in LC depth (2.3 μm/year, $P = 0.0035$) in the AD group. The sclera was thickest in the superior and temporal regions while the LC was thinnest superiorly.

Conclusions. Substantial sectorial and racial differences in LC and scleral morphology were observed, as well as increasing LC depth and scleral thickness with age in the AD group. Results suggest greater age-related remodeling of the load-bearing ONH connective tissues in eyes from AD individuals that could explain, in part, the greater predilection to glaucomatous injury seen in aged AD populations.

Keywords: lamina cribrosa, race, optic nerve head, morphometry

A variety of in vivo clinical observational and quantitative imaging studies have demonstrated differences in the structure of the optic nerve head (ONH) between individuals of African (AD) and European descent (ED).[1–10] It has been suggested that these differences may play a role in the increased susceptibility to glaucomatous injury seen in AD populations,[11] as differences in the morphology of any load bearing tissue can have significant impact on mechanical strain (local tissue deformation).[12–20] Furthermore, we recently used spectral-domain optic coherence tomography (SDOCT) to demonstrate that advancing age is associated with increased laminar surface depth in normal AD individuals[2] and eyes from normal AD individuals exhibit greater posterior deformation of the lamina cribrosa (LC) in response to acute intraocular pressure (IOP) elevation compared to normal ED individuals.[21] We have recently shown that peripapillary scleral structural stiffness increases with age in both AD and ED donor eyes, and advancing age.

We have also reported that peripapillary structural stiffness is significantly greater in older normal eyes of ED donors compared to younger ED donors, and varied by sector using scleral inflation tests.[22–24] When peripapillary scleral strain was measured in normal ED eyes and compared to AD eyes across age, the increase in age-related scleral stiffness in AD donor eyes was almost twice as large as that seen in ED eyes.[24] These changes were driven in part by age- and race-related differences in scleral material properties, which are independent of scleral thickness.[25] Computational models have demonstrated that the thickness[26,27] and depth[18] of the LC, along with the thickness of the peripapillary sclera,[18,26–28] are important morphologic features that influence the resultant strain within the microenvironment of the LC in response to IOP-related stress. Taken together, these findings indicate that morphologic and material

property differences in the ONH across racial groups may have an effect on the mechanical response of these tissues to IOP variations.

Unfortunately, current in vivo SDOCT imaging approaches lack the depth penetration necessary to fully visualize the collagenous load bearing structures of the ONH, other than a limited portion of the anterior laminar surface.[29] Few histologic studies have been performed examining racial differences in ONH morphology.[30,31] These studies utilized processing approaches that did not allow for accurate quantification of three-dimensional (3D) morphometry and were performed in eyes fixed at atmospheric pressure (zero IOP), which significantly alters ONH morphology.[32] Sigal and colleagues[33,34] developed an approach allowing for 3D quantifications of human donor eyes fixed at physiologic and elevated IOP. They demonstrated a wide variation in laminar and scleral morphology, but their cohort only included ED individuals.[34]

The purpose of the current study is to compare the 3D morphologic structure within high-resolution 3D digital reconstructions of the LC and peripapillary sclera of normal ED and AD eyes using 3D quantifications of high-fidelity episcopic fluorescent digital 3D ONH reconstructions. To do so, we obtained eyes fixed at physiologic IOP from AD and ED donors with clinical records available to confirm normality and fixed them at 10 mm Hg of manometrically controlled IOP.

Episcopic approaches, which have previously been used only in nonhuman primate eyes,[35–37] employ imaging of the embedded tissue block surface rather than slide-mounted histologic sections. In so doing, they minimize problems associated with warping and folding of tissue sections that have been mounted on glass slides prior to imaging for morphometry as done in prior studies.[33,34] Block face imaging also allows for alignment of serial sections with nanometer precision, eliminating misalignment that occurs with assuming that fiducial or anatomic markers used to stack serial sections are perfectly perpendicular to the section plane.[33,34] Block-face imaging also allows for high-resolution imaging at 1.5×1.5 μm pixel resolution every 1.5-μm section thickness across a large field of view (6.2×6.2 mm), thereby maximizing the resulting volume image resolution while capturing the entire ONH and peripapillary sclera in a single aligned volume. The fluorescent imaging approach utilized the intrinsic fluorescence of collagen, removes the need for staining, and allows for automation. The resulting digital 3D ONH volumes enable high-fidelity 3D delineation using simultaneous sagittal and transverse visualization in custom software.

Methods

Donor ocular tissues were obtained through the Alabama Eye Bank according to standard eye banking procedures. All donor eyes were obtained within 6 hours of death. Consent to utilize donor tissues for research was obtained from the next of kin from all study participants and all components of this study adhered to the tenets of the Declaration of Helsinki.

The certified tissue procurement technician conducted a structured interview with the next of kin to obtain the medical and ophthalmic history of the donor. This interview includes specific questions regarding a history of glaucoma, macular degeneration or other retinal disease, prior ocular surgeries, and central nervous system (CNS) disease. Donors whose family reported a history of retinal, optic nerve, or CNS disease were excluded from the study. The survey also assessed information regarding the identity and location of the donor's eye care provider and the consent to obtain this information was acquired. Any donor tissues in which the medical records were not available to confirm a normal eye exam (excluding cataracts and cataract extraction) were excluded from this analysis. We included 64 eyes from 51 donors in the current analysis, in which both eyes were immersion fixed at an IOP of 10 mm Hg; 13 donors had both eyes included. A total of 19 eyes were from donors of African descent and 45 eyes were from donors of European descent. The contralateral eyes from donors not used in this study were fixed at a higher IOP (45 mm Hg) as part of an addition study to examine the effect of IOP.

Both donor eyes were removed via enucleation by an experienced technician as follows. The conjunctiva was incised posterior to the limbal insertion of Tenon's fascia and undermined. The rectus muscles were disinserted with tenotomy scissors. The optic nerve was cut with scissors as far from the insertion to the globe as possible. Only pairs of eyes that were obtained within 6 hours of death and have at least 3 mm of optic nerve posterior to the scleral insertion were used. Any eyes with obvious external scleral pathology or injury from procurement that might affect the posterior sclera were not processed further.

Two sclerostomies were made with a 23-gauge needle inferotemporally, 1 mm apart at the level of the pars plana, 3 mm posterior to the limbus. Two self-retaining retinal infusion cannulas attached by intravenous tubing to a custom pressurization device described below were inserted into the vitreous cavity. The infusion line was attached to bottles of balanced salt solution (BSS) and the fixative solution through a 3-way stopcock. The drain line was attached to an IOP sensor and pressure control valve designed to maintain the IOP at 10 mm Hg level during processing and fixation. The sensor provides feedback to the valve to maintain a constant pressure within the eye. Two additional sclerostomies were performed superotemporally and superonasally using a 20-gauge blade (V-lance; Alcon Surgical, Fort Worth, TX, USA). The core vitreous and anterior vitreous skirts were removed using a vitrectomy hand piece (Alcon Surgical MVS XX, model 11–06503; Alcon Laboratories, Fort Worth, TX, USA) under direct visualization via an ocular endoscope (URAM E4, E4 Microprobe; EndoOptiks, Little Silver, NJ, USA). This procedure ensures that no residual vitreous remains in the region of the inflow and outflow cannulas that may interfere with adequate maintenance of IOP or flow of BSS/fixative into the vitreous cavity.

Once the vitrectomy was complete, the sclerostomies used for the endoscopic vitrectomy were occluded with scleral plugs and IOP was set to 10 mm Hg and maintained with balanced salt solution in both eyes for 30 minutes to allow equilibration, then a mixture of 2% glutaraldehyde and 1% paraformaldehyde in 0.1 M phosphate buffer at room temperature was infused into the vitreous cavity through the infusion line, slowly replacing the BSS solution while pressure was maintained. While the pressurization device maintains IOP at 10 mm Hg, the eyes are immersed in 2% glutaraldehyde and 1% paraformaldehyde to ensure full thickness fixation at the desired IOP. The processing and fixation of the fellow eye is performed concomitantly.

After 6 hours in fixative, the eyes were removed from the fixation chamber and the cannulas removed. The anterior segments were removed using scissors at the level of the pars plana and the posterior segments were submerged in 2% glutaraldehyde and 1% paraformaldehyde and left for 6 hours. The eyes were then sectioned at the equator and inspected for any sign of pathology such as macular or retinal scarring. Eye with gross retinal pathology were excluded.

Episcopic Digital Reconstruction

The optic nerve head and peripapillary sclera was separated from the posterior pole with an 8-mm-diameter trephine. The

Investigative Ophthalmology & Visual Science

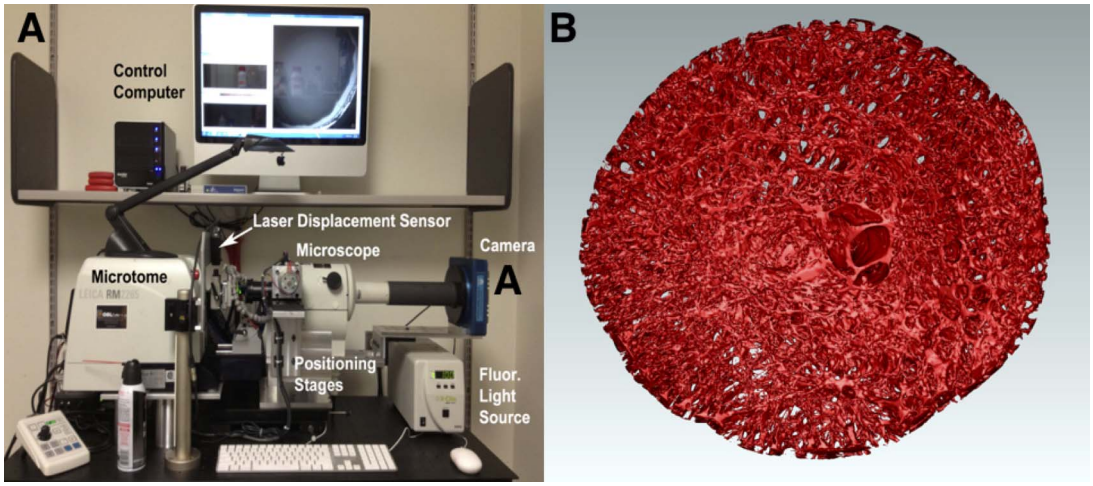

Figure 1. (**A**) Custom automated Episcopic Fluorescent Image Capture device (*right*) that is optimized to image the surface of the embedded ONH tissue block face at high resolution after each thin section is taken. Laser displacement readings of the block position taken after each section is cut allow automated alignment and stacking of the resulting serial block face images into a volumetric 3D ONH reconstruction. (**B**) En face (*anterior*) view of the segmented LC derived from a fluorescent 3D ONH reconstruction of a normal human donor eye. (**C**) A video of the reconstruction passing anteriorly from the vitreous side through the optic nerve and sclera is provided online as Supplementary Material.

specimens were photographed under a dissecting microscope, capturing images of the ONH and macula, and a small notch cut was made in the superior sclera for orientation. The trephined ONHs were then post-fixed in 5% glutaraldehyde for at least 48 hours to enhance tissue autofluorescence. The trephined ONH tissues were dehydrated through a series of graded ethanol baths, and triple cleared in HPLC chloroform using an automatic tissue processor (Sakura Tissue-Tek II; Ames Division, Miles Laboratories, Inc., Elkhart, IN, USA). Tissues were then infiltrated with a mixture of 50 mL chloroform and 0.25 g fat-soluble dye (Sudan IV dye, No. S4261; Sigma-Aldrich Corp., St. Louis, MO, USA), first under 400 mbar vacuum for 10 minutes, then at ambient atmospheric pressure for another 4 hours. The chloroform mixture was then pipetted off, and the specimens were infiltrated with a mixture of 25.0 g stearic acid (No. S4751; Sigma-Aldrich Corp.) and 1.0 g fat-soluble dye (Sigma-Aldrich Corp.) for 4 hours at 75°C under 400 mbar vacuum. Specimens were then placed in paraffin embedding molds and infiltrated in the embedding mixture of 10.0 g stearic acid; 1.6 g fat-soluble dye (Sigma-Aldrich Corp.); 72 g paraffin (65°C melting point, No. 41663; Sigma-Aldrich Corp.); and 14.8 g wax additive (Vybar 260; Candlewic, Inc., Doylestown, PA, USA) overnight at 75°C under 400 mbar vacuum. Finally, the embedding mixture infiltration solution was pipetted off, and the molds were refilled with the embedding mixture a second time after block chucks were fitted to the molds, and allowed to cool into paraffin tissue blocks. The embedding mixture has been optimized to block light across a broad spectrum, such that fluorescent imaging of the block face after microtome sectioning only captures those tissues exposed on the block face itself.[38,39]

The optic nerve tissue was then digitally reconstructed using an automated episcopic fluorescent reconstruction approach conceptually similar to that used previously in non-human primates studies on ONH morphology (Fig. 1).[40] In brief, this custom, microtome-based device allows for automated, high-resolution, three-dimensional, histologic reconstructions of ocular tissues in the fluorescent domain. The system is fully automated and is based on a commercial microtome (Leica RM-2265; Leica Biosystems, Buffalo Grove, IL, USA), which has been modified to section automatically under computer control. As the specimen is sectioned at 1.5-μm thickness, the cut block face is episcopically imaged with a Texas Red filter cube using a microscope (Nikon AZ-100; Nikon Instruments, Inc., Tokyo, Japan) fitted with a fluorescent light source (Ex-Cite 120 PC; EXFO Life Sciences & Industrial Division, Mississauga, Ontario, Canada) and a 12-bit grayscale camera (Alta U16M; Apogee, Andor Technology Ltd., Belfast, UK) with a 4096 × 4096-pixel CCD chip. The light-blocking agent (Sudan IV) limits fluorescent excitation/emission to only those tissues exposed on the embedded tissue block face surface, thereby minimizing photo bleaching and eliminating the need for image deconvolution. Optical resolution is set to 1.5 μm/pixel and verified with a slide-mounted micrometer scale, yielding a field of view of 6.2 × 6.2 mm, and serial images are captured after each 1.5 μm-thick section is cut from the block face. Images are automatically aligned using an laser displacement sensor (LK-G32; Keyence, Itaska, IL, USA), which measures the vertical stopping position of an optical-grade mirror (NT43–410; Edmund Optics, Barrington, NJ, USA) that is epoxied to the top of the block carrier to within 200 nm after each section is taken. Image acquisition, sectioning, and registration are automated in a fault tolerant Java-based control system, and approximately 1200 serial sections are included in each ONH reconstruction. The system thereby allows the capture of the entire ONH and a 2-mm-wide band of peripapillary sclera in a single 3D image volume at an isotropic voxel resolution of 1.5 × 1.5 × 1.5 μm.

Images were acquired beginning at the retina/vitreous interface, and taken until both the entire posterior scleral surface and at least 150 sections (225 μm) of the retrobulbar optic nerve posterior to the LC were acquired. Autofluorescent 3D ONH reconstructions of each eye were approximately 15 to 35 gigabytes in size depending on the number of section images acquired and stacked.

Visualization and Delineation

Reconstructions of the ONH were then visualized in custom software developed using the Visualization Toolkit (Multiview, Clifton Park, NY, USA). The approach to 3D delineation with the custom software (Multiview; Fig. 2) has been described in detail in prior publications.[35] In brief, the delineator selects the center of the neural canal as the approximate center axis of rotation through which all radial digital sagittal sections will be taken for delineation; this procedure is unique for every eye,

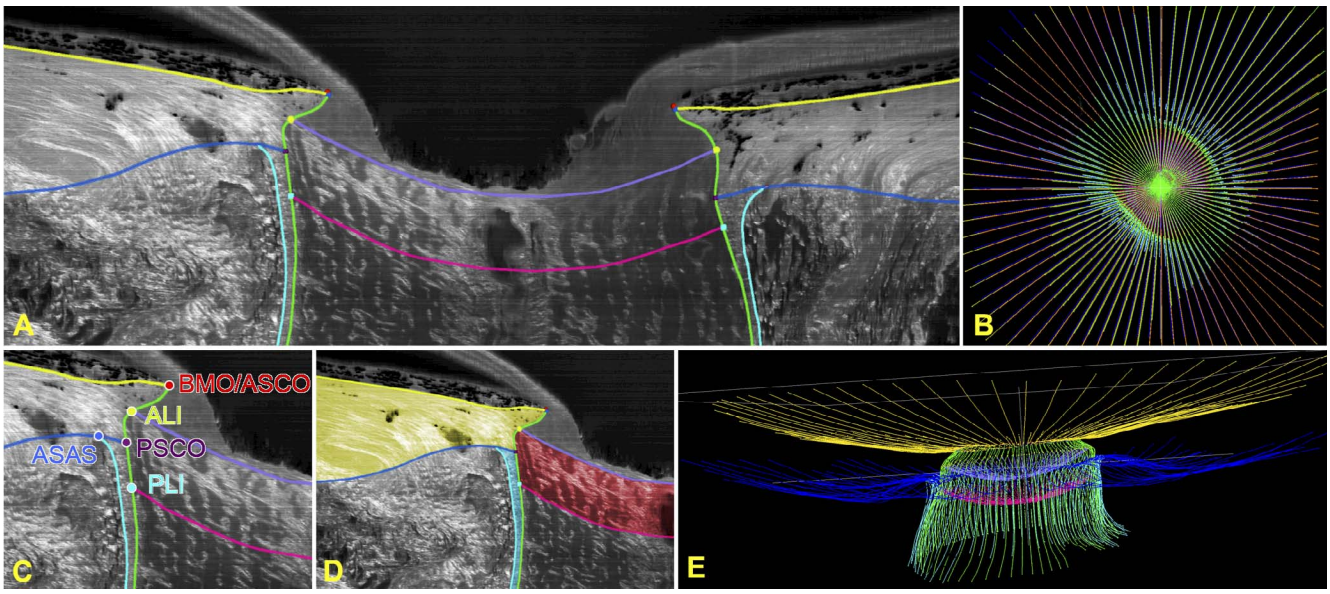

Figure 2. 3D delineation of principal anatomic surfaces and landmarks in the ONH. Our automated fluorescent 3D ONH reconstruction device is based on serially imaging the block face of a paraffin-embedded ONH specimen at 1.5 × 1.5 μm/pixel resolution using a episcopic fluorescent microscope fitted with a 16-megapixel, grayscale CCD camera after each 1.5-μm-thickness microtome section is cut. Approximately 1200 images for each ONH are precisely aligned into a fluorescent 3D ONH reconstruction using a nanometer-precision laser displacement sensor that records the specimen position for each image. Once the autofluorescent images are aligned and stacked to create a volume, we use custom delineation software to slice the volume along 40 radial sagittal planes centered on the ONH and delineate the principal anatomic surfaces using Bezier curves, and mark points for the landmarks that define the morphology of the ONH and peripapillary sclera as follows. (**A**) A single digital sagittal slice in which the anterior and posterior surfaces of the lamina and sclera, the neural boundary, and the exterior surface of the pia have been delineated with Bezier curves by placing a series of curve control points along the anatomic surface. (**B**) the transverse (*en face*) view of the radial Bezier curve delineations showing the 40 radial marking planes for each ONH. (**C**) A close-up view of the delineated ONH and scleral canal landmark points: BMO; ASCO (here coincident with BMO); the anterior laminar insertion (ALI); the anterior-most aspect of the subarachnoid space (ASAS); the PSCO; and the posterior laminar insertion (PLI). Note the BMO and ASCO landmarks are identical in this section on both sides of the canal, but that is not always the case. (**D**) The delineated surfaces define the areas of the sclera (*yellow*); lamina cribrosa (*red*); and pia (*light blue*) that are typically quantified. Note the partial insertion of the lamina into the pia on both sides of the canal. (**E**) View of the Bezier curve delineations for the full set of 40 radial marking planes for a human ONH.

and ensures that each radial section passes through the center of the ONH. The principle landmarks defining the morphologic surfaces of the ONH tissues are then manually delineated as previously described in 40 radial, 7-voxel thick sagittal sections taken around the center of rotation (Fig. 2). In each section, the observer delineates eight anatomic surfaces and six neural canal landmark points (Fig. 2). The surfaces delineated included the surface of the internal limiting membrane, Bruch's membrane, anterior and posterior scleral surfaces, anterior and posterior surfaces of the lamina cribrosa, the neural canal boundary and the boundary of the subarachnoid space.

Unlike prior 3D approaches used in human tissues,[33,34] the delineator can view both sagittal and transverse sections simultaneously, can scroll through the voxel planes composing each thick digital section, and tilt the sections within the reconstruction to better visualize surfaces of thin connective tissue features. This generates a 3D point cloud from which the morphometric quantifications are obtained. This enables more accurate delineation of the surfaces of the lamina cribrosa and sclera than two-dimensional (2D) approaches as illustrated in Figure 3. This is especially important in defining the posterior laminar boundary, which is difficult to visualize in sagittal sections alone, and for which a slaved transverse view proves necessary.

The retinal vasculature was reconstructed using the same software by delineating the major retinal vessels within transverse sections taken every 20 μm throughout the reconstruction. These vessel delineations were used to refine the alignment of the reconstruction to the ONH and macular fundus photos taken prior to episcopic reconstructions as shown in previous publications.[35–37] Once the alignment of the vessel and fundus photo was accomplished, fovea center and Bruch's membrane opening (BMO) centroid were identified and used to establish the fovea-BMO axis that serves as the clinical horizontal axis or nasal-temporal axis.[41] The regions of the LC and sclera were divided into four equal-area quadrants for analysis (superior, inferior, nasal and temporal) defined with respect to the fovea-BMO axis.

For each 3D ONH reconstruction, a least-squares ellipse was fitted to the marks defining the anterior scleral canal opening (ASCO) to create a reference plane (*X-Y* plane). Since BMO location may be related to choroidal thickness,[42] which is likely to differ in the postmortem setting due to the lack of blood pressure at the time of pressure fixation, ASCO was used as the reference plane. The center of the ASCO ellipse was used as the origin. All measurements of LC position were made relative to this plane. Depth of the anterior LC surface was calculated as the distance from the ASCO reference plane to the delineated surface along a vector normal to the ASCO reference plane sampled along a smoothed thin-plate B-spline surface (within ASCO reference plane or *X-Y* plane, LC surfaces were sampled on a 20 μm grid). The thickness of LC was calculated by fitting the anterior and posterior LC surfaces, as delineated by 2D B-spline curves in 40 radial sections, to continuous 3D surfaces with a thin-plate B-spline. Thickness was measured by creating a normal vector from the sampled smoothed LC anterior surface projected to the posterior LC surface on a 20-μm grid. Thus, thickness measurements are not subject to individual variation in density of manual measure-

Investigative Ophthalmology & Visual Science

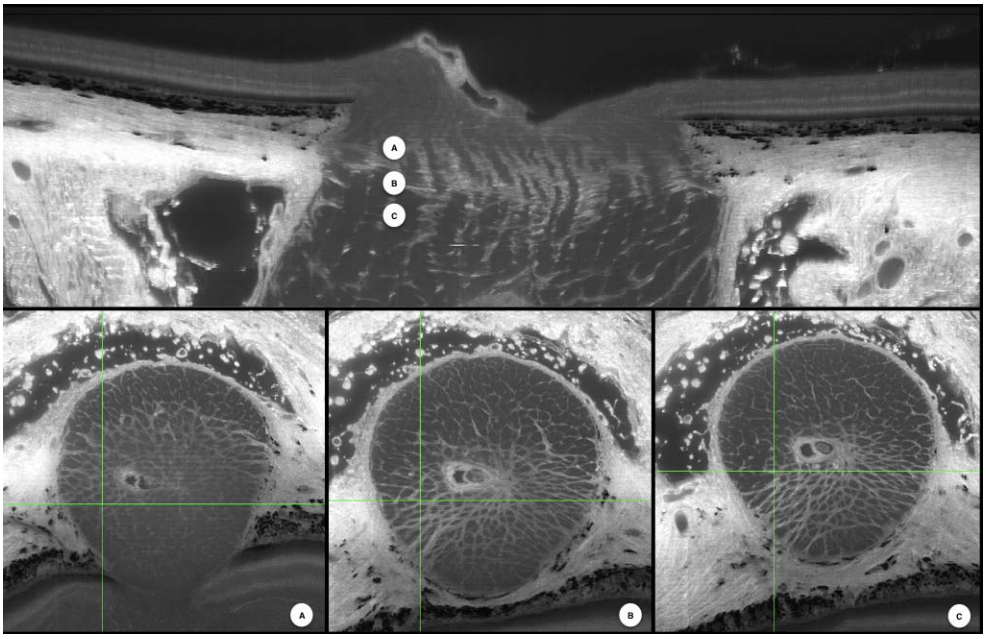

FIGURE 3. Sagittal (*upper*) and transverse (*lower*) images visualized simultaneously in the 3D delineation software (Multiview). Points (**A–C**) labeled in the sagittal image above correspond to the location of the *green crossbair* in the respective transverse images below, illustrating the position of the (**A**) anterior surface of the lamina cribrosa, (**B**) the middle of the lamina cribrosa, (**C**) and the posterior surface of the lamina cribrosa. Transverse images are digitally rotated 15° to facilitate visualization of the surface boundaries of the lamina cribrosa. Note the posterior boundary of the lamina cribrosa is clearly visible in the transverse section (**C**), but located much more posterior to the apparent posterior lamina that is visible in the sagittal digital section (*top*).

ments. The region occupied by the retinal vasculature within the lamina cribrosa was excluded from the measurement.

For the measurements of peripapillary scleral thickness, anterior scleral surface thin-plate and posterior scleral thin-plate B-spline surfaces were constructed from the 40 radial 2D-delineated B-splines from these structures. Thickness was measured by creating a normal vector from the smoothed anterior 3D scleral surface projected to the posterior scleral surface on a 20-μm grid. Scleral thickness data were then interpolated to generate continuous thickness, which allows resampling at any point. Scleral thickness was reported at 50-μm intervals for 40 resampled radials (4.5° apart) defined by the fovea-BMO axis, from the projected posterior scleral canal opening (PSCO) out to a maximum of 2200 μm from the BMO centroid.

Global and regional measurements of LC depth and thickness and scleral thickness were calculated and used in the analysis. The central and peripheral LC thickness was also quantified with the central region defined by 50% of the anterior laminar surface area centered on the centroid of the ellipse of the anterior laminar insertion. Data to define the reproducibility of the parameterization approach were determined by having the three trained delineators perform three repeated delineations of three separate volumes at least 2 weeks apart. All quantifications were done using custom software (MATLAB; MathWorks, Inc., Natick, MA, USA).

Statistical Analysis

Differences in regional and sectorial morphometric parameters were compared across racial groups by generalized estimating equations (GEEGLM package–R; Foundation for Statistical Computing, Vienna, Austria) adjusting for intradonor correlations of the regression residuals. Dependent variables used in individual models included regional and sectorial measurements of LC thickness, LC anterior surface depth and peripapillary scleral thickness. Variables explored in each model include age; race; sex; region of measurement; systemic disease (hypertension, diabetes); and the area of BMO and ASCO. For scleral thickness, we also included the radial distance (eccentricity) for the sampling points from the ASCO center in the model. Only covariates showing a significant association with the response variable were included in the statistical models; an interaction term between age and race was tested and included in the final model if significant. A value of $P < 0.05$ was considered as significant.

RESULTS

Donors of African descent were significantly younger than ED donors (49.4 versus 64.3 years old, $P < 0.001$). Therefore, all analyses were conducted controlling for age and interactions between age and race. These effects were left in the final models when significant. Donors of European descent had a similar prevalence of diabetes (AD = 10%, ED = 17.8%, $P = 0.4225$). Moreover, diabetes was not associated with any ONH morphometric parameter when included in the multivariable models, so it was excluded from the final models (lamina cribrosa thickness [LCT], $P = 0.9266$; scleral thickness, $P = 0.1526$; LC depth, $P = 0.3013$). Sex was independently associated with LCT and was included in the full model described below. Sex was not significant for scleral thickness or LC depth. Optic disc size, defined by ASCO average radius was significantly larger in the AD groups but did not vary with age (Table 1; Fig. 4). However, ASCO was not significant in any of the multivariable models (LCT, $P = 0.51768$; scleral thickness, $P = 0.7325$; LC depth, $P = 0.9334$) and thus was not included in any of the final models comparing associations with age and race.

Adjusting for age and sex, the LC was significantly thinner in eyes from AD donors compared to ED donors (difference in mean [AD – ED] = –23.9 ± 11.3 μm; $P = 0.0349$; Table 2).

Table 1. Results of Full Model for Regional and Racial Differences in Anterior Scleral Canal Opening Radius

Parameter (Reference)	Unit	Value	SE	*P* Value
Race (AD)	μm	70	23	0.0027
Nasal sector	μm	711	5	<0.001
Superior sector	μm	730	1	<0.001
Temporal sector	μm	704	5	<0.001
Inferior sector (intercept)	μm/year	732	10	<0.001

Inferior sector was the intercept.

Female sex was independently associated with a thinner LC (−24.0 ± 11 μm, $P = 0.0425$).

Box and whisker plots showing global racial differences and regional variation in LC thickness are shown in Figure 5. There was a similar pattern of regional variation of the LC across racial groups with the thinnest regions of the LC seen in the superior region (Figs. 5, 6). Age and BMO and ASCO area were not significantly associated with LC thickness in the univariate model or when included in the multivariable model and are not included in the final model.

Similar to LC thickness, the peripapillary sclera in eyes from AD donors was significantly thinner than in ED donors (Table 3; difference in mean [AD – ED] = −56 ± 22.0 μm, $P = 0.0097$). Scleral thickness increased with increasing eccentricity (in mm; 0.42 μm/mm, $P < 0.001$). However, including eccentricity in the full models did not affect the estimates in Table 3 so it was not included in the final models. A univariate model estimated a significant thickening of the sclera with age of 1.3 μm/year ($P = 0.0053$). A multivariate model accounting for sectorial variability and age-race interaction estimated a significant thickening of the sclera with age for the AD group of 1.3 μm/year ($P = 0.0499$), while the association was not significant for the ED group. Scatterplot and regression lines with 95% confidence intervals of the regression line are shown in Figure 7.

Sectorial variation in peripapillary scleral thickness was significant but showed a similar pattern across racial groups. The superior and temporal regions of the peripapillary sclera

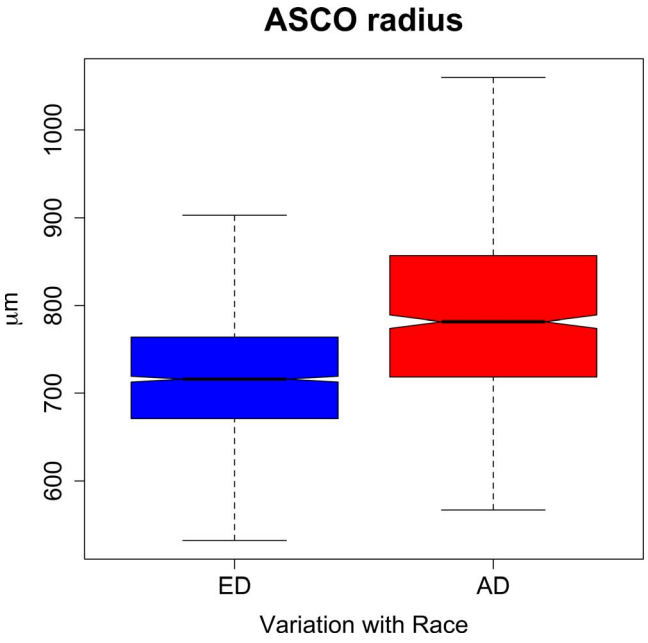

Figure 4. Difference in anterior scleral canal opening between eyes from AD and ED donors.

Table 2. Results of Full Model for Regional, Racial, and Sex Differences in LCT

Parameter (Reference)	Unit	Value	SE	*P* Value
Inferior sector (intercept)	μm	253	12.57	<0.001
Nasal sector	μm	248	3.69	0.20042
Superior sector	μm	236	4.64	0.00032
Temporal sector	μm	249	4.58	0.39841
Race (AD – ED)	μm	−23.9	11.3	0.03491
Sex, f	μm/year	−24.0	11.3	0.04254

Inferior sector was the intercept.

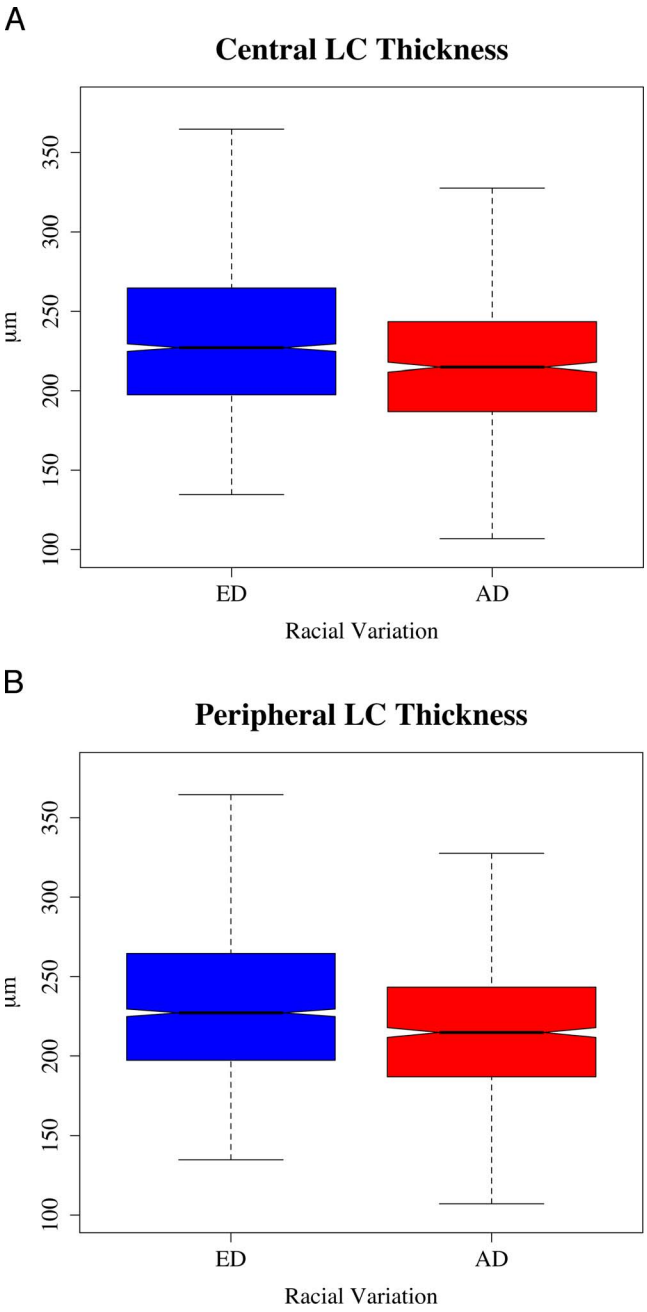

Figure 5. *Box and whisker* plots of the central and peripheral LC thickness determined from quantification of 3D ONH reconstructions in eyes from ED and AD donors.

Investigative Ophthalmology & Visual Science

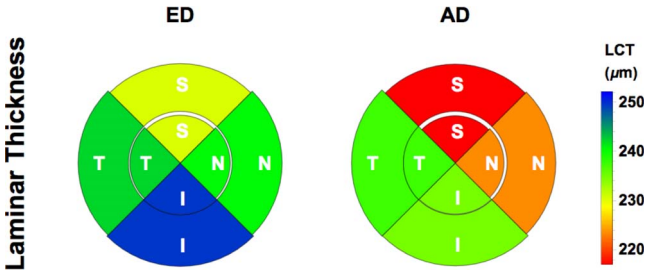

Figure 6. Regional and sectorial map of LCT determined from quantification of 3D ONH reconstructions in eyes from ED and AD donors. I, inferior; N, nasal; S, superior; T, temporal.

were significantly thicker than the inferior region, while the nasal region was the thinnest (Table 3). Figure 8 illustrates the differences in global and sectoral peripapillary scleral thickness. Age, sex, and BMO area were not associated with peripapillary scleral thickness in univariate correlations or the multivariable models and thus were not included in the final model.

The relationship between the depth of the lamina cribrosa, age, and race was more complex in the final model (Table 3). While there was not a significant change with age in the ED group, there was a significant interaction with race and age with a significant deepening of the lamina cribrosa with age in the AD group (2.3 μm/year, $P = 0.0035$). Thus, the model demonstrated a significantly shallower lamina cribrosa depth at younger ages in the AD group but a significantly deeper lamina cribrosa in the AD group at older ages (Table 4). Figure 8 shows a scatterplot illustrating the association with age in the AD and ED groups.

Measurement reproducibility was assessed by quantifying intra- and interobserver variability. The 3D morphology of four eyes was delineated by two observers as described above, and each observer repeated the delineation three times at least 2 weeks apart. The two-way random average intraclass correlation coefficient (Shrout and Fleiss formulation)[43] were 0.979 for LC depth, 0.87 for LC thickness, and 0.83 for scleral thickness. The 95% confidence interval for LC depth had a percent of variation of 2.7% with a measurement of uncertainty of 7.3 μm. For lamina cribrosa thickness, this was 8.2% (18.2 μm) and for scleral thickness, this was 4.7% (25.2 μm).

Discussion

This is first study to utilize episcopic 3D optic nerve reconstructions to quantify ONH and peripapillary scleral morphology in normal AD and ED human donor eyes and to utilize foveal-BMO axis for regionalization in human donor eyes to accurately characterize regional morphometric variation consistent with their in vivo orientation. Overall, the lamina

Table 3. Results of Full Model for Regional, Racial, and Age Differences in Thickness of the Peripapillary Sclera

Parameter (Reference)	Unit	Value	SE	*P* Value
Inferior sector (intercept)	μm	400	228	<0.001
Nasal sector	μm	379	5.0	<0.001
Superior sector	μm	472	6	<0.001
Temporal sector	μm	508	8	<0.001
Race, AD – ED	μm	−56.0	22.0	0.0097
Change with age/y (ED)	μm/year	0.6	0.7	0.364
Change with age/y (AD)	μm/year	1.3	0.7	0.0499

Inferior sector was the intercept.

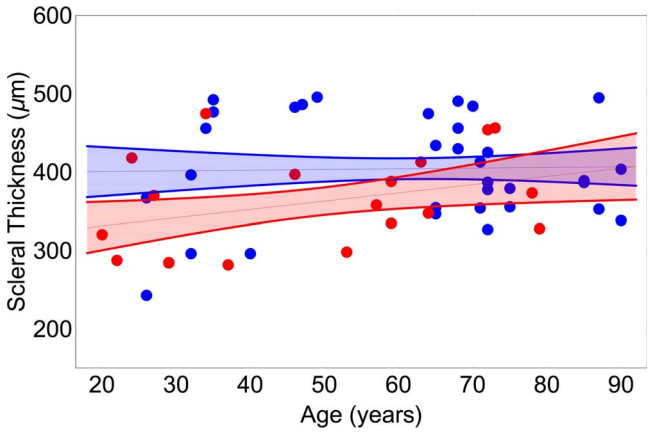

Figure 7. Scatterplots of the association peripapillary scleral thickness and age in eyes from donors of African (*red*) and European descent (*blue*). Mean and 95% confidence intervals (*shaded*).

cribrosa was significantly thinner in the superior sector when compared to the other sectors. Peripapillary scleral thickness was thinnest in the nasal sector, followed by the inferior, superior, and temporal sectors, listed in order of increasing thickness. Results demonstrate significant racial differences in the load-bearing connective tissues of the lamina cribrosa and peripapillary sclera. Specifically, the ONH from AD donors had a significantly thinner LC compared to ED donors. The peripapillary sclera was thinner with a shallower LC depth in the AD group at younger ages. Increasing age was associated with a thickening of the peripapillary sclera and a deeper LC in the AD group such that in LC depth was deeper in the older AD group. No age-related associations were seen in LC or peripapillary scleral morphology in the ED group. While these racial differences in ONH morphology may relate to group differences in the mechanical behavior of these tissues, there was wide variation in morphology and overlap between groups, indicating significant interindividual variability.

The findings of a thinner LC and peripapillary sclera in the AD group has important implications, as differences in the morphology of the ONH load-bearing connective tissues in individuals of African descent could potentially contribute to a greater deformability of the ONH. Prior work using simplified computational models assuming similar material properties, connective tissue density, and anisotropy suggest that the thinner LC and peripapillary sclera, along with a shallower LC depth would result in greater strain within these ONH tissues in response to IOP elevation, although these models did not use sectoral variations in LC or scleral geometry as shown herein, or include reported sectoral, age- and race-related differences in peripapillary scleral structural stiffness and material properties.[18,22,23,25–28,44] This hypothesis is intriguing given our prior in vivo work using SDOCT imaging in the African Descent and Glaucoma Study that has demonstrated greater deformations in the anterior LC surface in response to IOP elevations[21] and a more posterior location of the LC associated with normal aging and in AD individuals, with no aging effects seen in the ED group.[2] These in vivo SDOCT findings are corroborated by the ex vivo findings in the current study within high-resolution 3D ONH reconstructions that, unlike SDOCT, visualize the entire extent of the load-bearing connective tissues of the ONH. Taken together, these data suggest that the reported differences in the morphology of the load-bearing ONH connective tissues may, in part, define racial differences in the ONH biomechanical responses that drive the ONH remodeling that are an important component of aging and glaucomatous injury.[13,16] However, eye-specific biome-

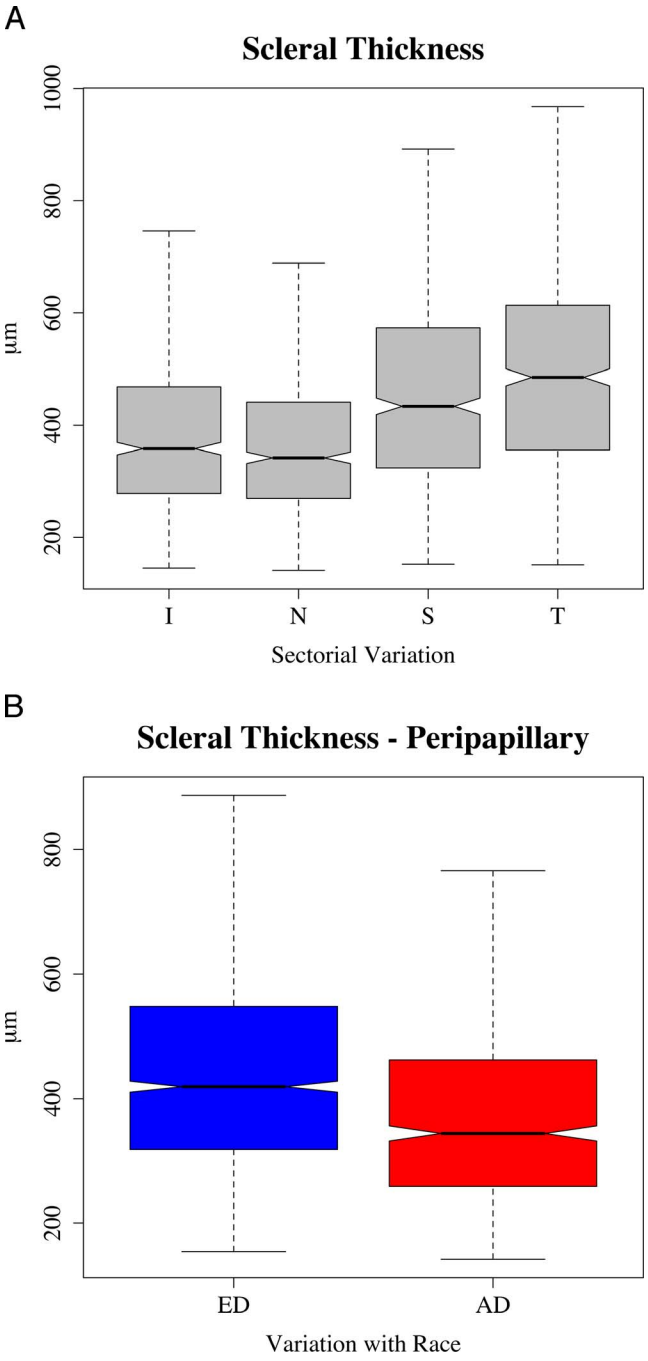

Figure 8. *Box and whisker* plots of global differences across racial groups (*left*) and sectorial differences (*right*) in scleral thickness determined from quantification of 3D ONH reconstructions in eyes from donors of ED and AD.

chanical modeling of the ONH would be useful in determining the effect of these age- and race-related differences in morphometry on ONH biomechanical behavior, and is a future direction of this work.[45–47]

Regional variation of LC and peripapillary scleral morphology was consistent across racial strata. The sclera was thickest in the superior and temporal sectors for both groups and thinner in the inferior and nasal sectors, while the LC was deepest and thinnest in the superior sector and thickest in the inferior sector in both racial groups. There is no prior literature examining regional variation in human LC thickness or depth

Table 4. Results of Full Model for Regional, Racial, and Age Differences in LC Depth

Parameter (Reference)	Unit	Value	SE	*P* Value
Inferior sector (intercept)	µm	251	19.1	<0.001
Nasal sector	µm	265	3.9	<0.001
Superior sector	µm	282	4.9	<0.001
Temporal sector	µm	250	3.8	0.78188
Change with age/y (ED)	µm/year	−0.6	0.7	0.41843
Change with age/y (AD)	µm/year	2.3	0.8	0.0035
Race (AD – ED, age 20 y)	µm	−113	43.7	0.00990
Race (AD – ED, age 60 y)	µm	3	24.2	0.91300
Race (AD – ED, age 90 y)	µm	90	44.9	0.0455

Inferior sector was the intercept.

in donor eyes and our study is the first to align the ONH based on the foveal-BMO axis. This ensures consistent alignment of the postmortem histology among all studied eyes and therefore allows for more anatomically accurate regional comparisons between individual donors. The biomechanical implications of this regional variation in the morphology of the LC and peripapillary sclera deserves further exploration with eye-specific computational modeling to determine sectoral mechanical strain distributions, but it is interesting that the thinnest sectors of the LC (superior) also corresponded to the deepest sectors, possibly indicating that these sectors are more vulnerable to posterior age-related remodeling.[48] In addition, the peripapillary sclera was thinnest in the inferior and nasal sectors, which likely results in higher strain in these areas within both the peripapillary sclera and the adjacent lamina at its insertion into the scleral canal wall.

The presented results also reveal a thinner LC in females compared to males independent of all other significant covariates. No prior study has demonstrated differences in LC thickness across sex. The effect of these differences on the vulnerability to glaucomatous injury is unclear. The Blue Mountain study demonstrated a higher prevalence of open angle glaucoma (OAG) in females[49] and the Rotterdam study demonstrated higher prevalence OAG in postmenopausal females.[50] These results were not adjusted for potential differences in IOP. Moreover, the prospective Collaborative Low Tension Glaucoma study also demonstrated higher rates of glaucoma progression in females.[51] In contrast, several other population-based studies have failed to show a higher prevalence of OAG in females.[52,53]

Previous methods used to define the connective tissue architecture of the human LC have employed standard histologic sectioning techniques with light and electron microscopy.[54–56] The approach used in this study fully reconstructs the connective tissue architecture of the ONH in 3D, allowing for the controlled digital sectioning needed for quantitative 3D histomorphometry. In addition, sectoral anatomy in the current study was aligned to the foveal-BMO axis, which should ensure greater correspondence of sectors measured histologically with the true in vivo position.

Limited histomorphometric studies have been performed examining racial differences in ONH connective tissues in postmortem donor eyes. Quigley et al.[57] performed a histologic study of 30 ED and 30 AD donor eyes and demonstrated a larger, more oval optic disc in the AD group. Additionally, Dandona and colleagues[31] examined seven ED and nine AD donor eyes using digital LC photography. They found an increase in the pore size in the superior and inferior poles of the ONH and an increase in the number of pores in the AD group.

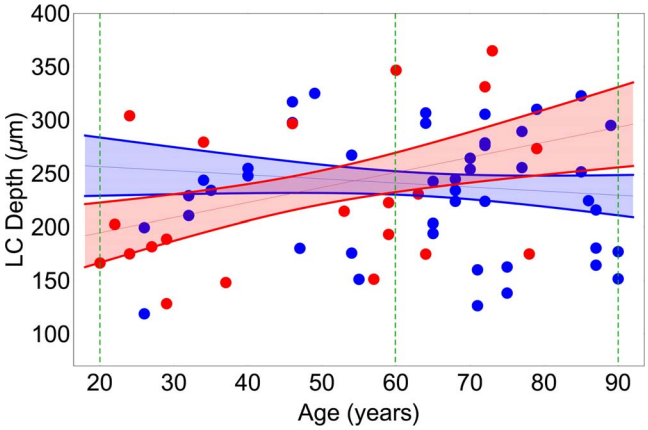

FIGURE 9. Scatterplots of the association of LC depth and age in eyes from donors of African (*red*) and European descent (*blue*). Mean (*line*) and 95% confidence intervals (shaded) of the regressions.

While prior studies using human tissue have demonstrated significant associations between variation in ONH morphology and African versus European ancestry, these prior studies have been limited to single histologic sections or images, which inadequately reflect the complex structure of the LC as a biomechanical structure and can lead to significant variation in LC appearance due to slight shifts in the orientation and position of the section plane. High-resolution 3D reconstruction of the ONH connective tissues is not possible using standard histologic techniques due to warpage and sectioning artifacts that prevent accurate section-to-section alignment of the tissues. Lastly, these studies were conducted in non-pressurized donor eyes. Significant conformational changes in LC structure can occur in the nonpressurized eye that will inaccurately reflect the in vivo anatomy in the pressurized human eye.[32]

Sigal et al.[33,34] developed a technique to process donor human tissue at pressure similar to our approach. Their 3D reconstruction approach utilized serial, vertically oriented sections through the ONH that are then aligned using embedded fiducial markers. When aligning the resulting images of stained sections mounted on glass slides, the images must be warped to realign the fiducial markers, and realignment inherently relies on the assumption that these markers are perfectly perpendicular to the section plane. Thus, these methods and their assumptions can lead to significant artifact in histologic slide-based 3D reconstructions and the resulting morphometric measurements.

The episcopic fluorescent image capture approach used in the current study images the embedded tissue block surface rather than standard cut sections, thus eliminating alignment and warpage problems associated with standard sectioning, while also allowing for much greater number of sections and much higher spatial resolution through the ONH. This greatly increases the volumetric image resolution and allows for 3D delineation with simultaneous visualization of two perpendicular 2D digital sections during manual delineation (Fig. 3). Furthermore, the current study, unlike any prior study using human ocular tissues, utilized only eyes confirmed to be normal based on their ophthalmic clinical records and direct next-of-kin interviews, and all eyes were collected within 6 hours postmortem, minimizing tissue degradation artifacts.

Of note, the study by Sigal et al.[34] reported a much thinner LC overall using their sagittal slide-mounted section approach when compared to the results reported herein. This may be due to the differences in the approach with delineation, as our 3D digital delineation approach allows the observer to mark points while simultaneously reviewing sections in two planes (sagittal and transverse). As illustrated in Figure 2, the posterior border of the LC is very difficult to mark accurately in a single sagittal section and is often located much more posteriorly than it appears. Sigal et al.[34] did not report any aging effects in their study, however, their donor population did not include AD subjects, and hence their findings are consistent with the results reported herein for the ED group.

This study has limitations common to studies using donor tissues. These include the cross-sectional nature of the study design, which limits the ability to draw definitive conclusions regarding the effects of aging on alteration or remodeling on the LC. However, this study is unique in that we only utilized tissue for which we acquired clinical records and direct interviews with next of kin that confirmed the presence of a normal eye exam prior to death, which provides a more certain classification compared to any prior work using donor tissues. Lastly, we only used donor tissue collected within 6 hours of death, which is a much more stringent collection window than has been used in other published studies, and helped ensure that postmortem tissue degradation is minimized to the extent possible.

There was an unequal age distribution among AD and ED donor that reflects the low participation of AD tissues available from eye donation. However, the multivariable analysis performed should be insensitive to the imbalance of age and should have effectively mitigated this disparity. To verify this, we performed an analysis truncated for age (range, 20–80 years; average: AD group, 51 years; ED group, 53 years). In this analysis, the effect of race remained significant with a modest shift in the estimated coefficients and a decrease in statistical significance.

It is possible fixation of the eye after enucleation may have altered the geometry of the ONH during since cerebrospinal fluid pressure in the subarachnoid space surrounding the optic nerve was zero. While this effect is unlikely to differ across age and race and therefore unlikely to alter the conclusions of the study, the position of the LC in this study may reflect a higher translaminar pressure gradient than is present at an IOP of 10 mm Hg in vivo. Moreover, the nerves were cut at least 3 mm posterior to the globe and eyes with any myelin extrusion were not reconstructed. We also pressurized the eyes to 10 mm Hg prior to fixation and held this pressure for 30 minutes to reduce any artifact due to harvesting of the tissues and the initial decompression of the eye after death. All tissues were treated identically in the study, but tissue shrinkage with fixation, dehydration, and embedding likely affects the reported absolute values of laminar and scleral thickness. It is possible that some of the reported age- or race-related differences in laminar and/or scleral morphometry could be due to differential differences in tissue shrinkage with processing. While prior studies in scleral tissue have shown little shrinkage from fixation, dehydration, and embedding,[58] it is possible that this could have affected the laminar morphometry reported herein if there are differences in laminar connective tissue volume fraction between racial groups.

In summary, the current study found large differences in the 3D histomorphometric measurements of LC and peripapillary scleral thickness between AD and ED groups using human donor tissues with confirmatory clinical records fixed at physiologic IOP. These include a significantly thinner peripapillary sclera and a thinner LC in AD individuals. The lamina cribrosa was also significantly shallower in young AD donors, but deepened with age. Moreover, this study provides preliminary evidence that age-related remodeling may occur to a greater extent in AD individuals, with increasing age being associated with a thicker peripapillary sclera and an increase in LC depth in eyes from AD but not ED donors. These

Investigative Ophthalmology & Visual Science

morphologic findings likely have significant effects on the biomechanical behavior of the ONH in response to IOP-related stress and may explain, in part, the greater predilection to glaucomatous injury observed in AD populations seen with advancing age. Future work involving eye-specific computational modeling using these high-resolution digital 3D reconstructions can estimate the biomechanical effects of the observed age- and race-related differences in the structure of the load bearing ONH connective tissues.

Acknowledgments

Supported by National Eye Institute (Bethesda, MD, USA) Grants R01EY018926 (JCD, CAG); R01EY019333 (JCD, CAG); and R21-EY018152 (JCD); Eyesight Foundation of Alabama (Birmingham, AL, USA); and a Research to Prevent Blindness Physician Scientist Award (New York, NY, USA; CAG).

Disclosure: **C.A. Girkin**, None; **M.A. Fazio**, None; **H. Yang**, None; **J. Reynaud**, None; **C.F. Burgoyne**, None; **B. Smith**, None; **L. Wang**, None; **J.C. Downs**, None

References

1. Girkin CA, Sample PA, Liebmann JM, et al. African Descent and Glaucoma Evaluation study (ADAGES): II. Ancestry differences in optic disc, retinal nerve fiber layer, and macular structure in healthy subjects. *Arch Ophthalmol*. 2010;128:541–550.
2. Rhodes LA, Huisingh C, Johnstone J, et al. Variation of laminar depth in normal eyes with age and race. *Invest Ophthalmol Vis Sci*. 2014;55:8123–8133.
3. Rhodes LA, Huisingh C, Johnstone J, et al. Peripapillary choroidal thickness variation with age and race in normal eyes. *Invest Ophthalmol Vis Sci*. 2014;56:1872–1879.
4. Varma R, Tielsch JM, Quigley HA, et al. Race-, age-, gender-, and refractive error-related differences in the normal optic disc. *Arch Ophthalmol*. 1994;112:1068–1076.
5. Beck RW, Messner DK, Musch DC, Martonyi CL, Lchter PR. Is there a racial difference in physiologic cup size? *Ophthalmology*. 1985;92:873–876.
6. Chi T, Ritch R, Stickler D, Pitman B, Tsai C, Hsieh FY. Racial differences in optic nerve head parameters. *Arch Ophthalmol*. 1989;107:836–839.
7. Tsai CS, Zangwill L, Gonzalez C, et al. Ethnic differences in optic nerve head topography. *J Glaucoma*. 1995;4:248–57.
8. Girkin CA, McGwin G Jr, Xie A, Deleon-Ortega J. Differences in optic disc topography between black and white normal subjects. *Ophthalmology*. 2005;112:33–39.
9. Girkin CA, McGwin G Jr, McNeal SF, DeLeon-Ortega J. Racial differences in the association between optic disc topography and early glaucoma. *Invest Ophthalmol Vis Sci*. 2003;44:3382–3387.
10. Girkin CA, McGwin G Jr, Long C, DeLeon-Ortega J, Graf CM, Everett AW. Subjective and objective optic nerve assessment in African Americans and whites. *Invest Ophthalmol Vis Sci*. 2004;45:2272–2278.
11. Girkin CA. Primary open-angle glaucoma in African Americans. *Int Ophthalmol Clin*. 2004;44:43–60.
12. Burgoyne CF. A biomechanical paradigm for axonal insult within the optic nerve head in aging and glaucoma. *Exp Eye Res*. 2011;93:120–132.
13. Burgoyne CF, Downs JC. Premise and prediction—how optic nerve head biomechanics underlies the susceptibility and clinical behavior of the aged optic nerve head. *J Glaucoma*. 2008;17:318–328.
14. Burgoyne CF, Downs JC, Bellezza AJ, Suh JK, Hart RT. The optic nerve head as a biomechanical structure: a new paradigm for understanding the role of IOP-related stress and strain in the pathophysiology of glaucomatous optic nerve head damage. *Prog Retin Eye Res*. 2005;24:39–73.
15. Downs JC. Optic nerve head biomechanics in aging and disease. *Exp Eye Res*. 2015;133:19–29.
16. Downs JC, Roberts MD, Burgoyne CF. The mechanical environment of the optic nerve head in glaucoma. *Optom Vis Sci*. 2008;85:425–435.
17. Sigal IA, Ethier CR. Biomechanics of the optic nerve head. *Exp Eye Res*. 2009;88:799–807.
18. Sigal IA, Flanagan JG, Ethier CR. Factors influencing optic nerve head biomechanics. *Invest Ophthalmol Vis Sci*. 2005;46:4189–499.
19. Cook R, Malkus D, Plesha ME, Witt RJ. *Concepts and Applications of Finite Element Analysis*. Hoboken, NJ: John Wiley & Sons, Inc.; 1989.
20. Hughes T. *The Finite Element Method*. Englewood Cliffs, NJ: Prentice-Hall, Inc.; 1987.
21. Fazio M, Johnstone J, Smith B, Wang L, Girkin C. Displacement of the lamina cribrosa in response to acute intraocular pressure elevation in normal individuals of African and European descent. *Invest Ophthalmol Vis Sci*. 2016;57:3331–3339.
22. Fazio MA, Grytz R, Bruno L, et al. Regional variations in mechanical strain in the posterior human sclera. *Invest Ophthalmol Vis Sci*. 2012;53:5326–5333.
23. Fazio MA, Grytz R, Morris JS, et al. Age-related changes in human peripapillary scleral strain. *Biomech Model Mechanobiol*. 2014;13:551–563.
24. Fazio MA, Grytz R, Morris JS, Bruno L, Girkin CA, Downs JC. Human scleral structural stiffness increases more rapidly with age in donors of African descent compared to donors of European descent. *Invest Ophthalmol Vis Sci*. 2014;55:7189–7198.
25. Grytz R, Fazio MA, Libertiaux V, et al. Age- and race-related differences in human scleral material properties. *Invest Ophthalmol Vis Sci*. 2014;55:8163–8172.
26. Sigal IA, Yang H, Roberts MD, et al. IOP-induced lamina cribrosa deformation and scleral canal expansion: independent or related? *Invest Ophthalmol Vis Sci*. 2011;52:9023–9032.
27. Sigal IA, Yang H, Roberts MD, Burgoyne CF, Downs JC. IOP-induced lamina cribrosa displacement and scleral canal expansion: an analysis of factor interactions using parameterized eye-specific models. *Invest Ophthalmol Vis Sci*. 2011;52:1896–1907.
28. Girard MJA, Downs JC, Bottlang M, Burgoyne CF, Suh JKF. Peripapillary and posterior scleral mechanics—part II: experimental and inverse finite element characterization. *J Biomech Eng*. 2009;131:051012.
29. Girard MJA, Tun TA, Husain R, et al. Lamina cribrosa visibility using optical coherence tomography: comparison of devices and effects of image enhancement techniques. *Invest Ophthalmol Vis Sci*. 2015;56:865–874.
30. Quigley HA, Brown AE, Morrison JD, Drance SM. The size and shape of the optic disc in normal human eyes. *Arch Ophthalmol*. 1990;108:51–57.
31. Dandona L, Quigley HA, Brown AE, Enger C. Quantitative regional structure of the normal human lamina cribrosa. A racial comparison. *Arch Ophthalmol*. 1990;108:393–398.
32. Bellezza AJ, Rintalan CJ, Thompson HW, Downs JC, Hart RT, Burgoyne CF. Anterior scleral canal geometry in pressurised (IOP 10) and non-pressurised (IOP 0) normal monkey eyes. *Br J Ophthalmol*. 2003;87:1284–1290.
33. Sigal IA, Flanagan JG, Tertinegg I, Ethier CR. Reconstruction of human optic nerve heads for finite element modeling. *Technol Health Care*. 2005;13:313–329.

34. Sigal IA, Flanagan JG, Tertinegg I, Ethier CR. 3D morphometry of the human optic nerve head. *Exp Eye Res*. 2010;90:70–80.
35. Yang H, Downs JC, Girkin C, et al. 3-D histomorphometry of the normal and early glaucomatous monkey optic nerve head: lamina cribrosa and peripapillary scleral position and thickness. *Invest Ophthalmol Vis Sci*. 2007;48:4597–4607.
36. Yang H, Downs JC, Bellezza A, Thompson H, Burgoyne CF. 3-D histomorphometry of the normal and early glaucomatous monkey optic nerve head: prelaminar neural tissues and cupping. *Invest Ophthalmol Vis Sci*. 2007;48:5068–5084.
37. Downs JC, Yang H, Girkin C, et al. Three-dimensional histomorphometry of the normal and early glaucomatous monkey optic nerve head: neural canal and subarachnoid space architecture. *Invest Ophthalmol Vis Sci*. 2007;48:3195–3208.
38. Rosenthal J, Mangal V, Walker D, et al. Rapid high resolution three dimensional reconstruction of embryos with episcopic fluorescence image capture. *Birth Defects Res C Embryo Today*. 2004;72:213–23.
39. Weninger WJ, Mohun T. Phenotyping transgenic embryos: a rapid 3-D screening method based on episcopic fluorescence image capturing. *Nat Genet*. 2002;30:59–65.
40. Burgoyne CF, Downs JC, Bellezza AJ, Hart RT. Three-dimensional reconstruction of normal and early glaucoma monkey optic nerve head connective tissues. *Invest Ophthalmol Vis Sci*. 2004;45:4388–4399.
41. Lockwood H, Reynaud J, Gardiner S, et al. Lamina cribrosa microarchitecture in normal monkey eyes part 1: methods and initial results. *Invest Ophthalmol Vis Sci*. 2015;56:1618–1637.
42. Johnstone J, Fazio M, Rojananuangnit K, et al. Variation of the axial location of Bruch's membrane opening with age, choroidal thickness, and race. *Invest Ophthalmol Vis Sci*. 2014;55:2004–2009.
43. Shrout PE, Fleiss JL. Intraclass correlations: uses in assessing rater reliability. *Psychol Bull*. 1979;86:420–428.
44. Fazio MA, Grytz R, Morris JS, Bruno L, Girkin CA, Downs JC. Human scleral structural stiffness increases more rapidly with age in donors of African descent compared to donors of European descent. *Invest Ophthalmol Vis Sci*. 2014;55:7189–7198.
45. Sigal IA, Grimm JL, Jan N-J, Reid K, Minckler DS, Brown DJ. Eye-specific IOP-induced displacements and deformations of human lamina cribrosa. *Invest Ophthalmol Vis Sci*. 2014;55:1–15.
46. Sigal IA, Flanagan JG, Tertinegg I, Ethier CR. Finite element modeling of optic nerve head biomechanics. *Invest Ophthalmol Vis Sci*. 2004;45:4378–4387.
47. Downs JC, Roberts MD, Burgoyne CF, Hart RT. Multiscale finite element modeling of the lamina cribrosa microarchitecture in the eye. *Conf Proc IEEE Eng Med Biol Soc*. 2009;2009:4277–4280.
48. Yang H, Williams G, Downs JC, et al. Posterior (outward) migration of the lamina cribrosa and early cupping in monkey experimental glaucoma. *Invest Ophthalmol Vis Sci*. 2011;52:7109–7121.
49. Mitchell P, Smith W, Attebo K, Healey PR. Prevalence of open-angle glaucoma in Australia. The Blue Mountains Eye study. *Ophthalmology*. 1996;103:1661–1669.
50. Hulsman CA, Westendorp IC, Ramrattan RS, et al. Is open-angle glaucoma associated with early menopause? The Rotterdam Study. *Am J Epidemiol*. 2001;154:138–44.
51. Drance S, Anderson DR, Schulzer M; for the Collaborative Normal-Tension Glaucoma Study Group. Risk factors for progression of visual field abnormalities in normal-tension glaucoma. *Am J Ophthalmol*. 2001;131:699–708.
52. Vajaranant TS, Nayak S, Wilensky JT, Joslin CE. Gender and glaucoma: what we know and what we need to know. *Curr Opin Ophthalmol*. 2010;21:91–99.
53. Higginbotham EJ. Does sex matter in glaucoma? *Arch Ophthalmol*. 2004;122:374–375.
54. Quigley HA, Addicks EM. Regional differences in the structure of the lamina cribrosa and their relation to glaucomatous optic nerve damage. *Arch Ophthalmol*. 1981;99:137–143.
55. Radius RL. Regional specificity in anatomy at the lamina cribrosa. *Arch Ophthalmol*. 1981;99:478–480.
56. Radius RL, Gonzales M. Anatomy of the lamina cribrosa in human eyes. *Arch Ophthalmol*. 1981;99:2159–2162.
57. Quigley H, Brown A, Morrison J, Drance S. The size and shape of the optic disc in normal human eyes. *Arch Ophthalmol*. 1990;108:51–57.
58. Olsen TW, Aaberg SY, Geroski DH, Edelhauser HF. Human sclera: thickness and surface area. *Am J Ophthalmol*. 1998;125:237–241.

Investigative Ophthalmology & Visual Science